Electrochemical appraisal of the Gemini surfactant as an inhibitor to reduce corrosion: simulation study to relate the inhibition efficiency with the electronic characteristics

M.J. Meften,[1] A.A. Kadhim,[1]* A.S. Abdulnabi[1] and J.M. Khalaf Al-zyadi[2]

[1]Department of Chemistry, College of Education-Qurna, University of Basrah, Basra 61001, Iraq
[2]Department of Physics, College of Education for Pure Sciences, University of Basrah, Basrah 6100, Iraq
**E-mail: ammar.kadhim@uobasrah.edu.iq*

Abstract

The current study included testing and evaluating the Gemini surfactant as an inhibitor to impart high resistance to corrosion challenges in installations used for seawater desalination, oil and gas transmission, and protection of down-hole pipelines (N-80 steel). The Gemini surfactant is sodium 2,2′-(18,25-dioxo-17,26-dioxa-20,23-diazadotetracontane-20,23-diyl) diacetate, designated as SDD. The SDD compound was studied as an inhibitor at 50°C (±1) in 1 N HCl as the corrosive environment. The inhibitor was evaluated through electrochemical impedance (EIS) and potentiodynamic polarization curves (PPC). The results showed that SDD acts as a mixed-type inhibitor. The theoretical adsorption characteristics were studied through the Monte Carlo technique, which provided useful information regarding the adsorption behavior of SDD, which adsorbed vertically on the Fe(001) surface through oxygen and nitrogen atoms. The simulation study confirms that the experimental results are associated with the electronic characteristics of the structure. The Gemini surfactant showed excellent results in inhibiting, where the efficiency optimum reached 89.40% and 91.37% as determined by the EIS and PPC techniques, respectively. From the Fermi level, it was noted that the minimum conduction band and the maximal valence band did not overlap, therefore metallic features appeared in the SDD inhibitor. Mulliken showed the electrophilic and nucleophilic sites, where the oxygen and nitrogen heteroatoms were the electrons-rich sites.

Received: September 24, 2024. Published: January 12, 2025 doi: 10.17675/2305-6894-2025-14-1-3

Keywords: *corrosion inhibitors, electronic characteristics, Tafel plot, Monte Carlo, HOMO, LUMO, SEM, EIS.*

1. Introduction

Carbon steel is widely used in the industry of production and transportation pipelines in oil facilities, therefore its corrosion causes tremendous damage to pipelines of crude oil transportation and thus threatens production and the global economy [1]. Recently, the use of surfactants as inhibitors has received extensive attention in the oil and gas industry for

corrosion inhibition of production and transportation pipes. The surfactant molecules usually adsorb on metal surfaces and form protective films that act as barriers to prevent penetration of corrosive environment and attack on the metal. Understanding the behavior of surfactants in corrosive environments is critical to their use as inhibitors. The oil and gas industry received considerable attention from researchers because oil mining and transportation have become expensive due to equipment damage caused by corrosive media containing H_2S, Cl_2, O_2, and CO_2 dissolved gases [2, 3]. The transportation of crude and refined petroleum depends mostly on the pipeline system. However, these pipelines are corroded by impurities and the presence of chromates, oxygen, carbon dioxide, and sulfur, which cannot be avoided. The organic inhibitors containing heteroatoms like S, N, O, *etc*., or polar functional groups were used as effective corrosion inhibitors [4–6].

Meanwhile, the challenges of the corrosion confrontation have important economic, technical, and environmental impacts, due to industrial use, particularly in the oil and gas production fields, and petrochemical industries. Inhibitors play an important role in decreasing corrosion by isolating and blocking the metallic surfaces from the corrosive environment, fashioning a protective hydrophobic film of adsorbed molecules on the metal surface [6–8]. Computational simulation is a useful method for analyzing the electronic parameters of the inhibitor's structure and enhancing the experimental results. The distribution of electrons in the HOMO and LUMO orbitals and the energy gap explain the adsorption phenomena and the inhibition mechanism of metal surfaces. Computational studies have become common in corrosion interpretation which helps understand and identify adequate sites for interaction between an inhibitor and a metal surface [9–11]. Three types of adsorption may occur on metal surfaces: (i) interaction between the metal and the free electron pairs of compounds, (ii) electrostatic attraction between the charged compounds and charged metal, (iii) interaction between a metal and π-electrons [12]. Almost all corrosion reactions of iron are electrochemical, where iron atoms undergo the oxidation process and turn into ions with liberation of electrons, where the negative charge quickly piles upon the metal and prohibits the anodic reaction [13]. The computational methodology confirmed the close correlation between inhibition efficiency and quantum properties like energy gap, highest occupied and lowest unoccupied molecular orbitals, and dipole moment [14, 15]. The Gemini surfactant *N*-(2-(((2-((dodecyldimethylammonio)oxy)ethyl)((26-hydroxy-3,6,9,12,15,18,21,24-octaoxahexacosyl)oxy) phosphoryl)oxy)ethyl)-*N*,*N*-dimethyl-dodecan-1-aminium bromide is a very effective inhibitor for corrosion of carbon steel [16]. To reduce the economic cost resulting from the extraction and transportation of crude oil, there must be inhibitors for the corrosion of crude oil pipes which is inevitable. The pipelines, wells, and tubing of oil wells are typically constructed of N80 steel, which is subject to significant rusting due to the aggressive nature of the acid solution during the pickling process. To mitigate metal loss during the process, corrosion inhibitors are added to the acid solution before the pickling process [17].

The Gemini surfactant (SDD) can treat the water in crude oil [18], therefore the main objective of this paper is to appraise the SDD as a practical corrosion inhibitor by the EIS

and PPC techniques and characterize it by theoretical study to get multiple uses for SDD, such as the treatment of water in crude oil, corrosion reduction of crude oil pipelines, with the corrosion reduction of installations' seawater desalination, and protection of down-hole pipelines.

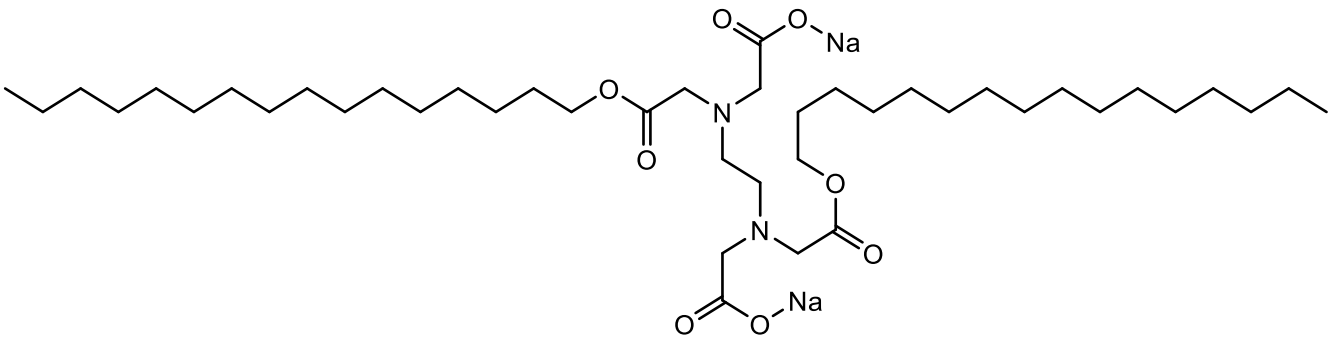

Figure 1. Chemical structure of the Gemini surfactant (SDD) [18].

2. Experimental Details

2.1. Synthesis of sodium 2,2'-(18,25-dioxo-17,26-dioxa-20,23-diazadotetracontane-20,23-diyl) diacetate

Step 1: Synthesis of ethylenediaminetetraacetic acid dianhydride (EDTA-DA).

EDTA dianhydride was synthesized by mixing 16 ml, 0.2 mol of pyridine with 14 ml, 0.15 mol of acetic anhydride. The mixture was added to 10 g, 0.34 mol of EDTA with stirring for 12 hrs. at 70°C. It was filtrated, washed with diethyl ether and dried. The yield was 86%.

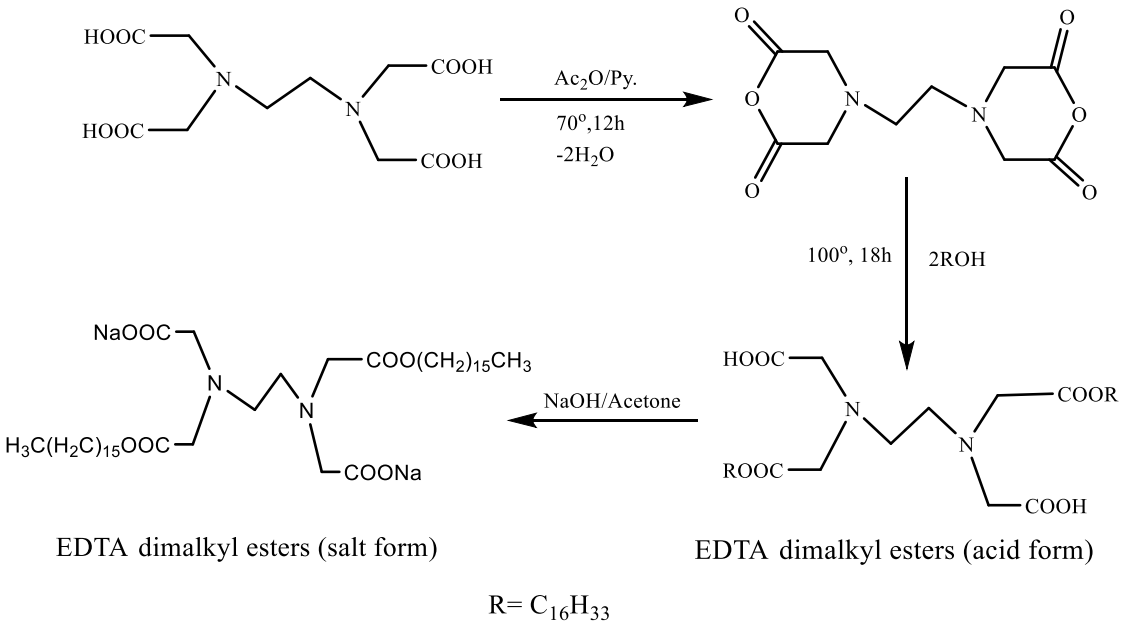

Figure 2. Synthesis sequence of the Gemini surfactant (SDD).

Step 2: Synthesis of EDTA dialkyl esters.

2.56 g, 0.01 mol of EDTA-DA prepared in step 1 was dissolved in 60 ml of DMF, then mixed with 4.84 g, 0.0002 mol of 1-hexadecanol at 100°C for 18 hrs. It was cooled at room temperature, and then 200 ml of an ice-water mixture was poured. A white substance that precipitated was then recrystallized from ethanol:water (2:5).

Step 3: Synthesis of sodium 2,2′-(18,25-dioxo-17,26-dioxa-20,23-diazadotetracotane-20,23-diyl) diacetate.

8%, 0.02 mol of NaOH was added to 0.01 mol of alcoholic solution of ester prepared in step 2 in batches at 25°C with continuous stirring, then 50 ml of acetone was added to it. The target compound precipitated as a white powder, then recrystallized from water:acetone (7:2) [18].

2.2. The experimental details of EIS, SEM, and PPC techniques

The EIS tests were carried out at 50°C in 1 N HCl as a corrosive solution in the presence of the inhibitor at 10, 20, 30, 40, and 50 mg/L concentrations. Electrochemical tests were performed in a three-electrode cell at a voltage of 20 mV *vs*. the open circuit potential and frequency ranging from 0.5 Hz to 100 KHz. The EIS characteristics obtained are the charge transfer resistance R_{ct}, solution resistance R_s, the potential of zero charge E_{pzc}, open circuit potential E_{ocp}, and double-layer capacitance C_{dl}. The R_s and R_{ct} were calculated using an electrochemical corrosion analyzer by intersecting the fitted semicircle with the real axis (Z_{real}) at the high and low frequencies, respectively. The C_{dl} was calculated by Equation 1 [19]. By reliance on Equation 2, the excess positive potential (E_p) was calculated [20]. The inhibitor efficiency (%) was calculated by Equation 3 [19].

$$C_{dl} = \frac{1}{\omega \cdot R_{ct}} \tag{1}$$

where ω is the angular frequency which equals $2\pi f_{max}$. Here, the f_{max} is the frequency in Hz.

$$E_p = E_{pzc} - E_{ocp} \tag{2}$$

The E_{pzc} and E_{ocp} represent the potential of zero charge and open circuit potential, respectively.

$$IE\%_{(EIS)} = \frac{R_{ct(inh)} - R_{ct(uninh)}}{R_{ct(inh)}} \cdot 100\% \tag{3}$$

The $R_{ct(inh)}$ and $R_{ct(uninh)}$ are the charge transfer resistance of the inhibited and uninhibited solution, respectively. The R'_{ct} represents the charge transfer resistance with diffusion layer resistance which was calculated as described in Equation 4 [21].

$$R'_{ct} = R_{ct} - R_s \tag{4}$$

The analysis of the N-80 surface was done using a scanning electron microscope (SEM) before and after immersion in 1 N HCl for 10 hrs. in the presence of 50 mg/L inhibitor at 50±1°C. After the samples were removed from the corrosive solution, they were rinsed with ethanol and dried, then inspected in a TESCAN VEGA3 instrument operated at an accelerating voltage of 30/20 kV.

To evaluate the SDD, it was studied as an inhibitor at different concentrations at 50°C in 1 N HCl by the potentiodynamic polarization curves (PPC) technique. Tafel curves were recorded on N-80 carbon steel with polarization potentials ranging from –250 to +250 mV relative to the open circuit potential at a scan rate of 1 mV/s. The solution volume in the corrosion cell was 500 ml. The reference electrode was Ag/AgCl. The PPC parameters that were identified from the Tafel plots included the corrosion potential (E_{corr}), corrosion current density (I_{corr}), and slope of the anodic and cathodic curves (β_a, β_c), respectively. The inhibitor efficiency, surface coverage, and displacement of corrosion potential ΔE_{corr} were calculated by Equations 5, 6, and 7 respectively [21, 22]. The constant phase element (CPE) Q_{ad} represented the adsorption capacitance and was calculated by Equation 8, where Y_0 and α are Z_{CPE} fit parameters, w is the angular frequency, and $j = \sqrt{-1}$ [23]. The polarization resistance P_R includes several types of resistance, electrolyte resistance, charge transfer resistance, film resistance, *etc*., [24] and was calculated by Equation 9 [25].

$$IE\%_{(PPC)} = \frac{i_{corr}^0 - i_{corr}}{i_{corr}^0} \cdot 100\% \tag{5}$$

$$\theta = \frac{i_{corr}^0 - i_{corr}}{i_{corr}^0} \tag{6}$$

where i_{corr}^0 and i_{corr} are corrosion current densities in the absence and presence of an inhibitor, respectively.

$$\Delta E_{corr} = E_{corr} - E_{corr}^0 \tag{7}$$

where E_{corr} and E_{corr}^0 denoted the corrosion potential with and without inhibitor, respectively.

$$\mathrm{CPE} = Y_0^{-1}\left(jw\right)^{-\alpha} \tag{8}$$

$$P_R = \frac{\beta_c \cdot \beta_a}{2.3 i_{corr}\left(\beta_c + \beta_a\right)} \tag{9}$$

The composition of N-80 steel (wt%) is C, 0.31; Mn, 0.92; Si, 0.19; S, 0.008; P, 0.010; Cr, 0.20 and remainder Fe.

3. Results and Discussion

3.1. Surface characterization by scanning electron microscopy (SEM)

Scanning electron microscopy is a technique that is important for providing information about the surface morphology, topography, and products of the corrosion process [26]. To evaluate the conditions of the N-80 surface and determine whether an inhibitor protected the surface of N-80, the carbon steel was immersed in the corrosive environment for 10 hours, and then analyzed immediately after removal from the corrosive environment. The microscopic image of the uninhibited surface revealed that there are distortions and several pits generated due to an aggressive HCl attack on the N-80 surface as shown in Figure 3b. Despite this, a microscopic image of the surface in the presence of 50 mg/L of SDD shows that surface corrosion decreased remarkably and possesses fewer distortions (smoother compared with that in the absence of the inhibitor), as shown in Figure 3c [27–29]. This indicates and confirms that the carbon steel surface is fully covered by the adsorbed inhibitor molecules, furthermore a protective inhibitor film was formed on the surface of N-80, revealing the inhibition of carbon steel corrosion by the SDD inhibitor [30].

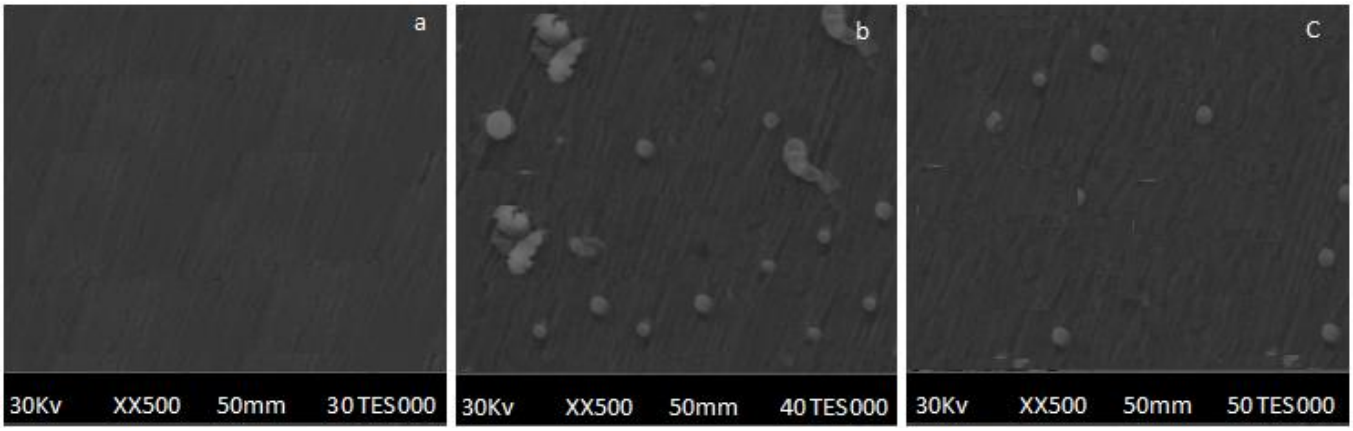

Figure 3. SEM images of carbon steel: (a) polished surface, (b) in 1 N HCl without inhibitor for 10 h, (c) in 1 N HCl containing 50 mg/L of SDD for 10 h.

3.2. Results of EIS

The SDD was studied with the EIS technique most precisely. The Nyquist plots in the absence and presence of the inhibitor reveal that the diameter of the semicircle in the absence of the SDD is smaller than in its presence, as shown in Figure 4. The plots obtained in the presence of SDD are made up of regular semicircular capacitive loops. It was seen that the capacitive loop in the presence of the inhibitor has a diameter larger than in the absence of the inhibitor, which proves that carbon steel's impedance rises with the addition of the SDD to the corrosive environment [31, 32]. The semicircles in the Nyquist plot were observed as incomplete, due to dispersion, deviation of frequency, distortions, and inhomogeneity of the carbon steel surface [32]. An increase in the SDD concentration led to a growth in the diameter of the semicircle in the curve. This finding implies that charge transfer resistance

increased and the corrosion rate decreased. The Nyquist plots show depressed semicircular arcs at high and intermediate frequencies. The width of the capacitive loop in the curve widens as the inhibitor concentration increases, indicating effective adsorption and better protection, as shown in Figure 4 [33, 34].

The benefit of Bode plots is that they provide confirmed information on the relation of real impedance with the frequency [35]. The Bode plots show that an increase in SDD concentration led to a broad shift in the impedance modulus, indicating a delay in the corrosion process [31]. The highest real impedance was noted at the lowest frequency, and the level of corrosion inhibition was high at 89.40%, and the lower the frequency, the more efficiently the SDD increased. This suggests the creation of a protective film from the SDD to shield the surface of carbon steel to be most stable as shown in Figure 5 [35]. The impedance increased in the presence of the inhibitor compared to that without an inhibitor (blank) due to prevention of the corrosion process [36]. Of the concentrations used, the higher concentration of 50 mg/L provided the highest impedance at the lowest frequency. Thus, these results confirm that the best inhibition was reached at 50 mg/L [36].

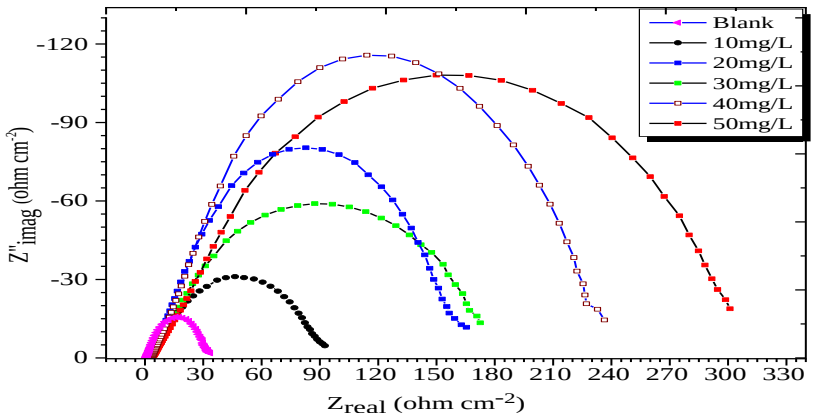

Figure 4. Typical Nyquist plots in the uninhibited solution and in the solutions inhibited by SDD.

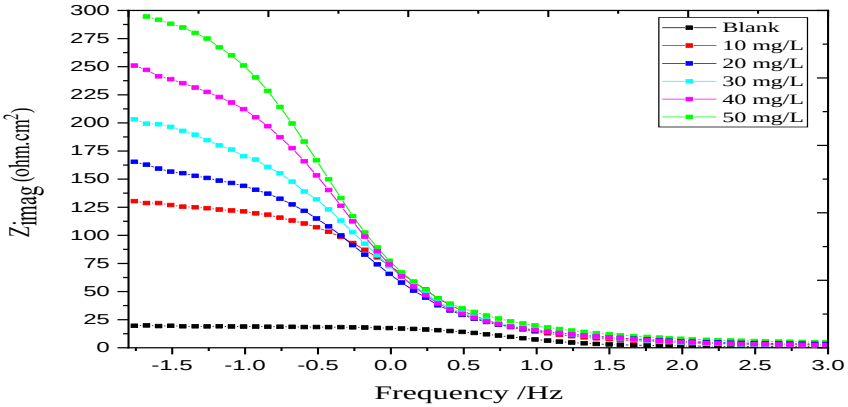

Figure 5. Bode plots in the uninhibited solution and in the solutions inhibited by SDD.

Table 1 demonstrates that the values of charge transfer resistance R_{ct} increased greatly with an increase in the concentration of the SDD inhibitor. This possibly indicates that the protective layer is formed on the carbon steel surface, which created barriers for charge transfer and prevented corrosion. At the highest value of R_{ct} 301.00 $\Omega \cdot cm^2$, the ratio of protection against corrosion was excellent and amounted to 89.40% [34, 36]. In contrast, the obvious decrease in double-layer capacitance accompanied by a regular increase in charge transfer resistance is a likely a consequence of the adsorption of the SDD molecules on the N-80 surface. In this regard, the adsorption leads to an increase in the adsorbed film thickness, a decrease in the local dielectric constant, or both. This case was attributed to the fact that the adsorbed molecules of SDD with a lower dielectric constant gradually replaced H_2O molecules on the surface of carbon steel [37, 38].

Table 1. Results of EIS in the inhibited and uninhibited solutions by SDD at 50°C (±1).

Conc. (mg/L)	f_{max} **(Hz)**	C_{dl} **(μF/cm²)**	R_{ct} **(Ω·cm²)**	R_s **(Ω·cm²)**	R'_{ct} **(Ω·cm²)**	***EI*** **(%)**	**α**	$Q_{ad}\cdot10^{-3}$ **($s^{\alpha}/\Omega\cdot cm^2$)**
0	112.3	44.74	31.88	0.21	31.67	–	1.973	2.224
10	60.27	28.94	91.29	0.79	90.50	65.07	0.745	1.756
20	44.50	21.63	165.40	1.23	164.17	80.72	0.612	1.002
30	42.44	21.75	172.50	1.69	170.81	81.51	0.782	0.732
40	31.06	21.68	236.40	2.231	234.16	86.51	0.699	0.664
50	28.54	18.53	301.00	3.237	297.76	89.40	0.792	0.298

According to the Helmholtz model, the better inhibition performance of the SDD inhibitor is associated with the Q_{ad} value. The element α represents a gauge to determine the surface inhomogeneity resulting from roughness and the adsorption of the inhibitor molecules on it. The decrease in Q_{ad} values from $1.756\cdot10^{-3}$ $s^{\alpha}/\Omega\cdot cm^2$ at 10 mg/L to $0.298\cdot10^{-3}$ $s^{\alpha}/\Omega\cdot cm^2$ at 50 mg/L suggests an increase in the thickness of the electrical double layer due to the adsorption of SDD molecules on the carbon steel surface by replacing SDD molecules rather than water molecules. It is worth noting that the experimental results showed that the efficiency increases with decreasing Q values as shown in Table 1 [39, 40]. The values of (OCP) and (PZC) without inhibitor are 88.81 mV/SCE and 125.71 mV/SCE respectively, while in 50 mg/L the values are 103.5 mV/SCE and 225 mV/SCE respectively. The E_{pzc} value is more positive than the OCP, hence the charge of the N-80 surface (E_p) is positive: +36.9 mV without the inhibitor and +121.5 mV with the inhibitor, so negative ions adsorb firstly on the surface [37]. When comparing the Gemini surfactant *N*,*N*′-((1,4-phenylene bis(azanediyl))bis(2-hydroxypropane-3,1-diyl))bis(*N*,*N*′dimethyldecan-1-aminium) (PAPM) with SDD in the current study, it was noted that the optimum efficiency of PAPM reached 90.32% for the weight loss method and 87.17% for the EIS technique [5]. The SDD

efficiency optimum reached 89.40% and 91.37% according to the EIS and PPC techniques, respectively.

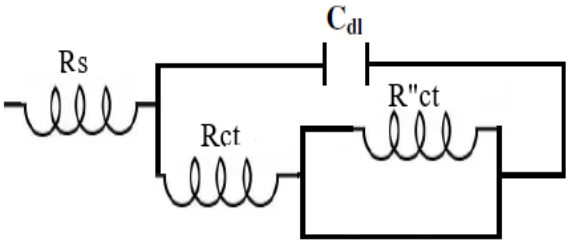

Figure 6. The equivalent circuit for fitting the EIS plots.

3.3. Potentiodynamic polarization curves (PPC)

Figure 7 shows the potentiodynamic polarization curves of carbon steel corrosion in 1 N HCl at different concentrations of the SDD inhibitor. From these curves, the corrosion current density was noted to decrease with an increase in the Gemini surfactant concentration due to the adsorption of the SDD molecules on the carbon steel, leading to a reduction in the metal dissolution rate due to the blanketing of the surface of N-80 and blocking the corrosive material from reaching the surface [41, 42]. In addition, a significant reduction was seen in the corrosion current density for all added concentrations compared to that obtained without the inhibitor. This may be due to the adsorption of the SDD molecules on the N-80 surface, thus blocking its active site [43]. The anodic slope (β_a) value is greater than the cathodic slope (β_c) value at all the concentrations. This implies that the presence of SDD hinders the dissolution N-80 more than hydrogen evolution [42]. There is a small shift in β_a values from 98 $mV \cdot dec^{-1}$ to 89 $mV \cdot dec^{-1}$ which is attributed to the formation of a protective layer of SDD that blocks the active centers and hinders the corrosion process [44]. The inhibition efficiency increases with an increased concentration of the inhibitor due to increased adsorption of the SDD inhibitor on the surface of carbon steel. The polarization resistance P_R which includes electrolyte resistance, charge transfer resistance, and film resistance, increased from 1.568 $\Omega \cdot cm^2$ to 2.010 $\Omega \cdot cm^2$, leading to increased inhibition efficiency from 78.48% to 91.37%. The surface coverage for N-80 increased with an increase in the concentration of SDD as shown in Table 2. The optimum inhibitor concentration is 50 mg/L and the inhibition efficiency obtained is 91.37% [42]. If the shift in the corrosion potential exceeds 85 mV compared to the corrosion potential in the inhibitor's absence, the inhibitor behaves as an anodic or cathodic type. In contrast, it is considered mixed inhibition if the potential change is less than 85 mV. Accordingly, the SDD represents a mixed-type inhibitor because the shift in corrosion potential is less than 85 mV as visible in Figure 7 and Table 2, therefore the SDD prevents both the cathodic and anodic processes together [41, 42, 44].

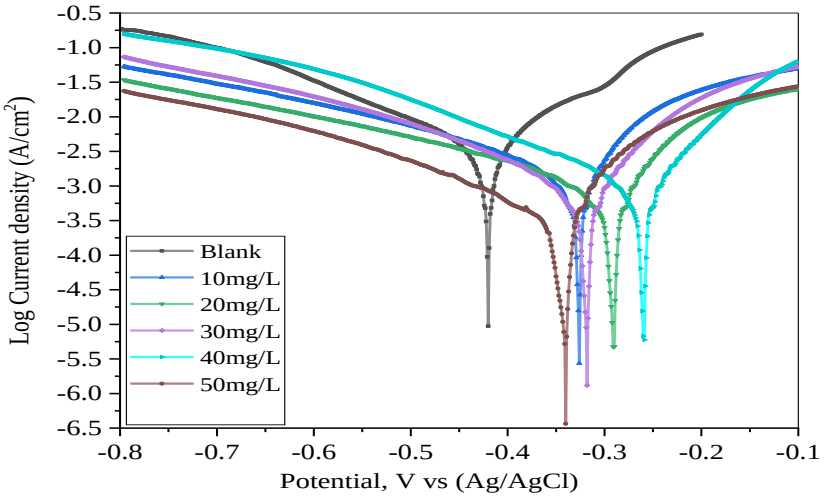

Figure 7. Typical Tafel plots in the uninhibited solution and in solutions inhibited by the SDD.

Table 2. Results of PPC in the uninhibited solution and in solutions inhibited by the SDD at 50°C (±1).

Concentration (mg/L)	E_{corr} (V/AgCl)	i_{corr} (mA·cm^{-2})	ΔE_{corr} (V)	β_a (mV·dec^{-1})	β_c (mV·dec^{-1})	P_R Ω·cm^2	θ	*IE*%
0	–0.421	54.75	–	104	–95	0.394	–	–
10	–0.326	11.78	0.095	98	–75	1.568	0.7848	78.48
20	–0.291	6.34	0.130	96	–43	2.036	0.8842	88.42
30	–0.318	5.98	0.103	92	–22	1.290	0.8907	89.07
40	–0.292	4.94	0.129	94	–35	2.244	0.9097	90.97
50	–0.340	4.72	0.161	89	–29	2.010	0.9137	91.37

4. Theoretical Investigation of the Performance of Gemini Surfactants

In general, the electronic characteristics can provide valuable information about the mechanism of inhibition and predict the adsorption of inhibitory materials on metal surfaces. They are considered as powerful tools for the analysis of experimental data and for investigating the interaction of the inhibitor with the surface of a metal. The electronic characteristics were analyzed by the DMol^3 Energy/EPS software [45], which included electrostatic potential surfaces (EPS), Mulliken charges, Fermi level, and HOMO, LUMO orbital values. In this regard and according to the energy values of the E_{HOMO} and E_{LUMO} orbitals, the energy gap (ΔE), electronegativity (χ), softness (s), ionization energy (IE), electron affinity (EA), hardness (η), chemical potential ρ, number of transferred electrons (ΔN) and $\Delta E_{Back\text{-}donation}$ were calculated. The energy gap and electronegativity were calculated by Equations 10 and 11, respectively [24].

$$\Delta E_{gap}=E_{LUMO}-E_{HOMO} \quad (10)$$

$$\chi=\frac{E_{HOMO}+E_{LUMO}}{2} \quad (11)$$

Ionization energy *IE* and electron affinity *EA* were calculated by Equations 12 and 13, respectively [46].

$$IE=-E_{HOMO} \quad (12)$$

$$EA=-E_{LUMO} \quad (13)$$

The softness (*s*) [47] and hardness (η) [48] were calculated by Equations 14 and 15, respectively.

$$s=\frac{1}{\eta} \quad (14)$$

$$\eta=\frac{IE-AE}{2}=\frac{\Delta E_{gap}}{2} \quad (15)$$

Chemical potential represents the first derivative of energy and was calculated through Equation 16 [37].

$$\rho=-\chi \quad (16)$$

The number of transferred electrons was calculated through Equation 17 [22, 34].

$$\Delta N=\frac{(\chi_{Fe}-\chi_{inh})}{2(\eta_{Fe}-\eta_{inh})} \quad (17)$$

where χ_{Fe} is the absolute electronegativity of iron, and χ_{inh} denotes the absolute electronegativity of inhibitor molecules, while η_{Fe} denotes the absolute hardness of iron and η_{inh} denotes the absolute hardness of inhibitor molecules.

In this regard, the χ_{Fe} equals 7 eV, and η_{Fe} equals 0 eV, and depending on these facts the ΔN can be calculated through Equation 18 [49].

$$\Delta N=\frac{7-\chi_{inh}}{2(\eta_{inh})} \quad (18)$$

As for the $\Delta E_{Back\text{-}donation}$, it was calculated through the relation with global hardness as shown in Equation 19 [50]:

$$\Delta E_{Black\text{-}donation}=\frac{-\eta}{4} \quad (19)$$

4.1. Electronic characteristics methodology

The energy of the Highest Occupied Molecular Orbital (HOMO) and Lowest Unoccupied Molecular Orbital (LUMO) are highly important properties closely related to each other, therefore they must be interpreted [51]. The high value of the HOMO indicates that the molecule has a strong tendency to donate electrons. In contrast, the low value of the LUMO refers to the ability to accept electrons and form stable bonds. The results of SDD molecules revealed that the value of HOMO and LUMO are −6.05 eV and −2.43 eV, respectively. The electronic configuration of the iron atom is $[Ar]^{18}$ $4s^2$ $3d^6$. The 4s orbital is occupied while the 3d orbit is unoccupied. Therefore, the 3d orbit can accept the electrons from the nitrogen and oxygen atoms in the inhibitor molecule using HOMO energy to relate the inhibitor molecule with the iron surface. The adsorption occurs through the formation of coordinate covalent bonds. Hence the iron surface behaves as an electrophile center while the hetero atoms in the SDD behave as nucleophile centers, so inhibition occurs [37, 51]. The SDD molecules can accept the electrons by the LUMO orbit from the anti-bonding orbit 4s of iron to form a back-donation bond with a value of −0.452 eV [24]. Furthermore, perhaps another inhibition occurs due to the interaction between the π-electrons of the SDD inhibitor and the d-orbit of the N-80, which increases the adsorption of the inhibitor molecules onto the iron surface to form a protective layer [37]. The HOMO and LUMO outcomes indicate that the electronic distribution density on the negatively charged oxygen and nitrogen atoms are the most favored locations for the inhibitor's adsorption through donor-acceptor bonds between the inhibitor and iron surface, respectively, as shown in Figure 8 [49]. Soft molecules possess a small value of ΔE_{gap}, and vice versa. Hard molecules are less reactive than soft molecules due to the large gap between the last occupied orbital and the first virtual orbit. The value of ΔE_{gap} is 3.62 eV, therefore the SDD molecules are soft and the occupied orbit will be low and more reactive with the iron surface due to the small gap. Furthermore, the band gap represents the stability of the SSD structure. The fraction of electrons refers to the transfer of electrons from the inhibitor to the metal if $\Delta N > 0$, while if $\Delta N < 0$, the electrons are transferred from the metal to the inhibitor. Inhibition efficiency increases as the electron transfer to the metal surface increases [52–54]. The value of ΔN is 0.76 eV and is larger than zero, therefore electrons are transferred from the SDD molecule to the N-80 surface, which enhances inhibition due to better electron exchangeability (Table 3) [48]. The hardness refers to the potential chemical change over the total number of atoms and its increase enhances the molecules' stability, while softness is a measure of the electron cloud polarization [49]. The hardness and softness are 1.81 eV and 0.55 eV, respectively. Hence, there will be polarization for nitrogen and oxygen electrons of the inhibitor on the surface of N-80. The ionization energy is the energy required to remove an electron of an inhibitor molecule at 6.05 eV, while the electron affinity is 2.43 eV [52].

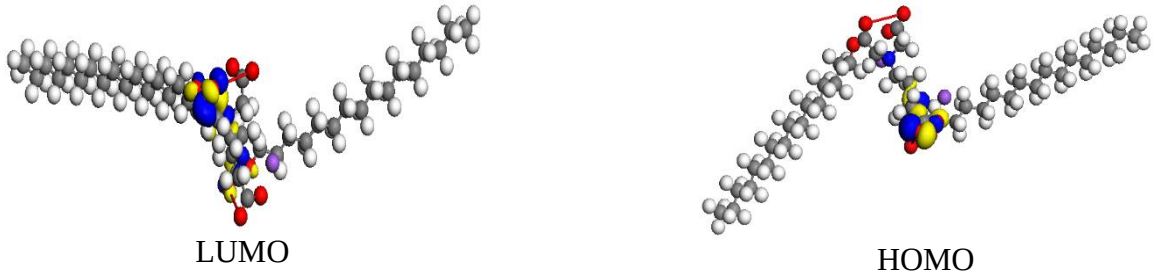

Figure 8. HOMO and LUMO orbitals of the Gemini surfactant.

Table 3. Electronic characteristics of the Gemini surfactant.

Quantum chemical parameter	Values
HOMO	–6.05 eV
LUMO	–2.43 eV
Energy gap (ΔE_{gap})	3.62 eV
$\Delta E_{Back\text{-}donation}$	–0.452
Number of transferred electrons ΔN	0.76
Electronegativity (χ)	4.24 eV
Softness (s)	0.55 eV
Hardness (η)	1.81 eV
Ionization energy (IE)	6.05 eV
Electron affinity (EA)	2.43 eV
Chemical potential (ρ)	–4.24 eV

4.2. Mulliken charge population

Almost all studies refer to the close relationship between the inhibition efficiency and Mulliken charge distribution of molecules. Previous studies showed that atoms bearing negative charges will donate electrons easily to the LUMO orbital of the metal atoms [55, 56]. Furthermore, the reaction of the atom site increases with an increase in the negative charge. Consequently, the atoms that have a pronounced negative charge in the Gemini surfactant will act as the active sites through which the inhibitor adsorbs onto the metallic surface of Fe. Indeed, the results obtained conclusively showed that the negative charges in red color concentrated on the N_{121}, N_{122}, and O_{123} atoms are the active sites (electrophilic attack) in the Gemini surfactant, as shown in the electrostatic potential surface (EPS), Figure 9. Where the deeper the color, the larger the degree to which electrons are accepted or donated. The bold values in Table 4 indicate the positive and negative charges of the main atoms that belong to the active regions which assist in the corrosion inhibition *via* absorption [55, 57]. The Mulliken charges were determined for the three most positive and three most

negative atoms in the Gemini surfactant. Clearly, N_{121}, N_{122}, and O_{123} are the most negative with values of −0.002, −0.013, and −0.026, respectively. In contrast, the most positive atoms are C_{22}, H_{55}, and Na_{132} corresponding to +0.153, +0.228, and +0.217, respectively. These results provided direct insights into electrophilic and nucleophilic sites. The oxygen and nitrogen heteroatoms are the electron-rich sites that can readily provide electrons needed to form a coordination bond. The positive charges were all identified on carbon atoms and sodium which are good sites for electrophilic reactions [58]. Generally, effective inhibitors contain O and N atoms.

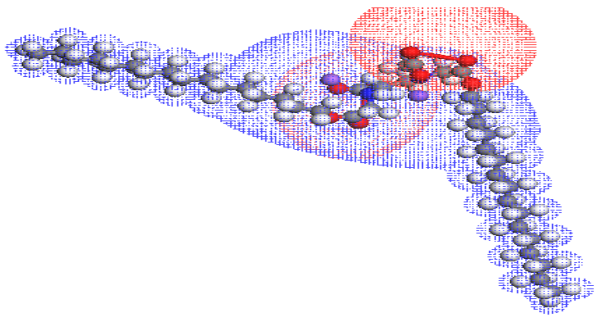

Figure 9. The electrostatic potential surface (EPS) of the Gemini surfactant. The red region shows an increase of electrons, while the blue area exhibits a lack of electrons.

Table 4. Mulliken atomic charges of the Gemini surfactant.

Atoms	Charge	Atoms	Charge	Atoms	Charge	Atoms	Charge	Atoms	Charge
C1	0.078	C31	0.027	H61	0.027	H91	0.027	N121	−0.002
C2	−0.003	C32	0.027	H62	0.027	H92	0.027	N122	−0.013
C3	0	C33	0.027	H63	0.027	H93	0.027	O123	−0.026
C4	−0.009	C34	0.027	H64	0.027	H94	0.027	O124	0.027
C5	−0.002	C35	0.027	H65	0.027	H95	0.027	O125	0.027
C6	−0.007	C36	0.027	H66	0.027	H96	0.027	O126	0.027
C7	−0.008	C37	0.027	H67	0.027	H97	0.027	O127	0.027
C8	0.027	C38	0.027	H68	0.027	H98	0.027	O128	0.027
C9	0.027	C39	0.027	H69	0.027	H99	0.027	O129	0.027
C10	0.027	C40	0.027	H70	0.027	H100	0.027	O130	0.027
C11	0.027	C41	0.027	H71	0.027	H101	0.027	Na131	0.016
C12	0.027	C42	0.027	H72	0.027	H102	0.027	Na132	+0.217
C13	0.027	H43	0.027	H73	0.027	H103	0.027		
C14	0.027	H44	0.027	H74	0.027	H104	0.027		
C15	0.027	H45	0.027	H75	0.027	H105	0.027		

Atoms	Charge	Atoms	Charge	Atoms	Charge	Atoms	Charge	Atoms	Charge
C16	0.027	H46	0.027	H76	0.027	H106	0.027		
C17	0.027	H47	0.027	H77	0.027	H107	0.027		
C18	0.027	H48	0.027	H78	0.027	H108	0.027		
C19	0.027	H49	0.027	H79	0.027	H109	0.027		
C20	0.027	H50	0.027	H80	0.027	H110	0.027		
C21	0.027	H51	0.027	H81	0.027	H111	0.027		
C22	+0.153	H52	0.027	H82	0.027	H112	0.027		
C23	0.027	H53	0.027	H83	0.027	H113	0.027		
C24	0.027	H54	0.027	H84	0.027	H114	0.027		
C25	0.027	H55	+0.228	H85	0.027	H115	0.027		
C26	0.027	H56	0.027	H86	0.027	H116	0.027		
C27	0.027	H57	0.027	H87	0.027	H117	0.027		
C28	0.027	H58	0.027	H88	0.027	H118	0.027		
C29	0.027	H59	0.027	H89	0.027	H119	0.027		
C30	0.027	H60	0.027	H90	0.027	H120	0.027		

4.3. Fermi level and partial density of states

The density of states DOS is based on the distribution of the molecular orbital energy levels. The results refer to the relative heights of the curves in different energy regions of SDD, implying that most molecular orbitals in the system have high energy. The electron transfer process strongly affects the molecules' adsorption of the Gemini surfactant on the iron surface. Figure 10 shows the partial density of states (PDOS) of the active positions in the inhibitor molecules. The adsorption of inhibitor molecules through the active groups in the Gemini surfactant was analyzed, and the DOS peaks of the *s* and *p* orbitals of the inhibitor shifted to lower energy. The s and p orbitals' peak positions in SDD were slightly changed. This refers to the adsorption of inhibitor molecules on carbon steel surfaces to enhance the inhibition. According to the results for the SDD, the E_{LUMO} and the E_{HOMO} are close to the Fermi level of Fe and are −0.0668 eV and −0.1985 eV, respectively. Under this situation and according to the results mentioned earlier, more electrons are likely to transfer from the HOMO orbital of the SDD molecule to the Fe surface, however, more electrons are likely to transfer from the Fe surface to the LUMO orbital of the SDD molecule. Therefore, the SDD molecules will accept and donate electrons, so the bonding intensity of the Gemini surfactant molecules with the Fe surface increases. This is beneficial to the displacement of water away from the Fe surface and also helpful for decreasing the number of water molecules in the compact layer [59, 60]. Hence, the charge-transfer resistance will increase, which agrees with the results of the EIS technique which reached 301.00 $\Omega \cdot cm^2$, and also the corrosion

rate will decrease significantly. Thus the SDD inhibitor shows an excellent inhibition [59, 60]. After the comprehensive analysis of the electronic properties of the SDD, it was noted that the bands did not surpass the Fermi level. However, the minimum conduction band and the maximal valence band did not overlap, therefore metallic features appeared in the SDD inhibitor. This conduct is seen in Figure 10 [61], demonstrating its strong metallic inhibition characteristics.

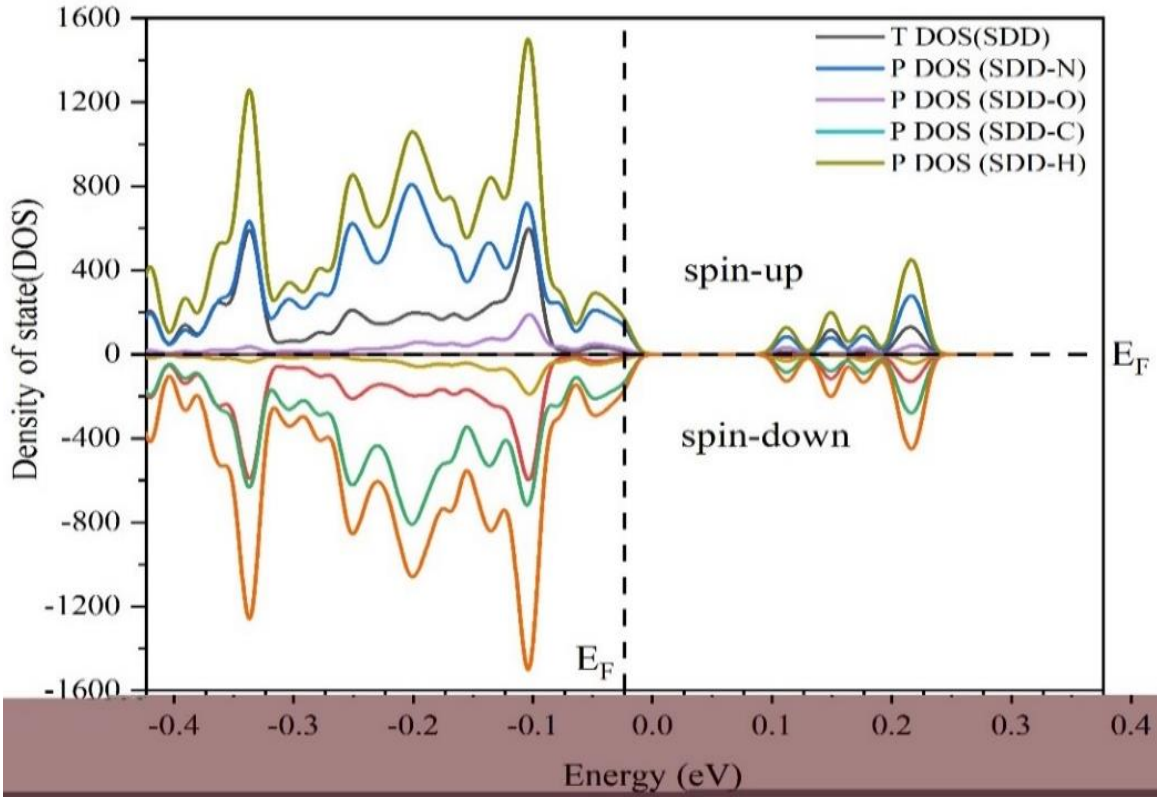

Figure 10. Fermi levels set at 0 eV and represented by vertical and horizontal dashed black lines.

4.4. Monte Carlo simulation (MCs)

The MCs method is considered very helpful in interpreting the adsorption process and the most stable adsorption sites over metal surfaces with low energy [53]. Figure 11 shows the electron transfer behavior, with adsorption configuration and difference in electron density of SDD atoms when adsorbed on Fe(001) surface. It is seen that the optimized structure of SDD molecules vertically adsorbs on the Fe(001) surface *via* oxygen and nitrogen heteroatoms at different distances from the N-80 surface, while the hydrophobic alkyl chain is away from the Fe(001) surface at different angles as shown in Figure 11. These results indicate that the adsorbed atoms are same sites of electrophilic attack shown in each of the Mulliken charges and electrostatic potential surface EPS [60, 62, 63].

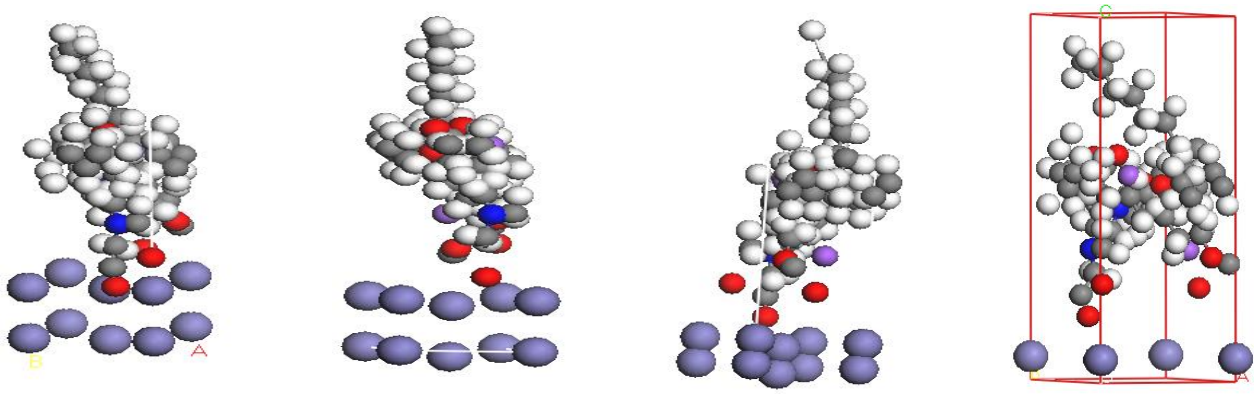

Figure 11. The adsorption of SDD by heteroatoms at different distances and angles from the Fe(001) surface monolayer.

5. Conclusions

The study conclusions are that the theoretical results corroborated the experimental results on the corrosion inhibition of N-80. The optimum efficiency is 91.37% and 89.40% at 50 mg/L of SDD according to the PPC and EIS techniques, respectively. In the Fermi level, the DOS peaks of the s and p orbitals of the SDD shift to lower energy. The PPC results revealed that the SDD is a mixed-type inhibitor. The choice of corrosion inhibitors is based on the active groups in the chemical structure, type of adsorption, cost, and environmental effect. The Gemini surfactant molecules have multiple applications such as treatment of water in crude oil and reduction of corrosion. The MCs method confirmed that SDD molecules adsorb vertically on the Fe(001) surface *via* the oxygen and nitrogen atoms, in contrast, the hydrophobic alkyl chain is away from the Fe(001) surface at different angles. The Mulliken charge showed that the negative charges concentrated on N_{121}, N_{122}, and O_{123} atoms, which are considered more active sites to donate electrons in the SDD inhibitor. The C_{dl} value decreases significantly with the addition of the SDD inhibitor, indicating that the thickness of the adsorbed film on the N-80 surface depends on the concentration of the inhibitor. EIS curves exhibited regular capacitive loops, and corrosion of N-80 steel was controlled *via* increasing the SDD concentration, which increased the charge transfer resistance. SEM showed a smoother microscopic image of the N-80 surface in the presence of the inhibitor, which decreased the surface corrosion remarkably. Metallic compounds have a high inhibition characteristic. Soft molecules are better than hard molecules in the inhibition.

Funding

Our research did not receive any specific grant from funding agencies in the public, commercial, or not-for-profit sectors.

Conflicts of Interest

The authors declare they don't have competing financial interests that affect scientific work in this paper.

References

1. Y. Zhu and M.L. Free, Electrochemical measurement and modeling of corrosion inhibition efficiency of surfactants in salt solutions, *Electrochem. Soc*., 2015, **66**, no. 17, 53–72. doi: 10.1149/06617.0053ecst
2. Y. Zhu, M.L. Free, R. Woollam and W. Durnie, A review of surfactants as corrosion inhibitors and associated modeling, *Prog. Mater. Sci*., 2017, **90**, 159–223. doi: 10.1016/j.pmatsci.2017.07.006
3. B. Brycki and A. Szulc, Gemini surfactants as corrosion inhibitors. A review, *J. Mol. Liq*., 2021, **344**, 117686. doi: 10.1016/j.molliq.2021.117686
4. V. Saraswat, T.K. Sarkar and M. Yadav, Evaluation on corrosion mitigation capabilities of nitrogen-doped carbon dots as corrosion inhibitors for mild steel in descaling solution, *Mater. Chem. Phys*., 2024, **313**, 128678. doi: 10.1016/j.matchemphys
5. M.J. Meften, Gemini surfactant performance evaluation as inhibitive action of PAPM for treatment of AISI steel corrosion and studying temperatures influence in acidic medium, *UTsci*., 2019, **7**, no. 1, 103–112. doi: 10.32792/utq/utjsci/v7i1.260
6. M.J. Meften, Synthesis, characterization and study of a new heterocyclic compound a corrosion inhibitor in 15% HCl solution, *Int. J. Innov. Res. Sci. Eng. Tech*., 2016, **5**, no. 7, 13685–13696. doi: 10.15680/IJIRSET.2016.0507227
7. A.S. Fouda, A.M. Eldesoky, F.S. Mohamed and M.W. El-Sherbeni, Electrochemical and quantum chemical Investigations of some cyanoacetamide derivatives as eco-friendly corrosion inhibitors for aluminum-silicon alloy in acidic solution, *Int. J. Electrochem. Sci*., 2017, **12**, no. 5, 4134–4149. doi: 10.20964/2017.05.10
8. M. Akgul, H. Gerengi, O. Camlibel and M. Sahun, Investigation of corrosion pattern of AISI 316 and AISI 304 stainless steels in $Na_2B4O_7 \cdot 5H_2O$ solution, *Int. J. Corros. Scale Inhib*., 2017, **6**, no. 1, 70–81. doi: 10.17675/2305-6894-2017-6-1-6
9. O. Sikemi, O.A. Kolawole and S. Banjo, Quantum chemical studies on corrosion inhibition of 1,3-thiazine derivatives for mild steel in acidic media: DFT Approach, *Manila J. Sci*., 2017, **10**, 44–63.
10. A. Kokalj, On the alleged importance of the molecular electron-donating ability and the HOMO–LUMO gap in corrosion inhibition studies, *Corros. Sci*., 2021, **180**, 109016. doi: 10.1016/j.corsci.2020.109016
11. N.O. Obi-Egbedi and I.B. Obot, Xanthione: A new and effective corrosion inhibitor for mild steel in sulphuric acid solution, *Arabian J. Chem*., 2013, **6**, no. 2, 211–223. doi: 10.1016/j.arabjc.2010.10.004

12. A.R.H. Zadeh, I. Danaee and M.H. Maddahy, Thermodynamic and adsorption behavior of medicinal nitramine as a corrosion inhibitor for AISI steel alloy in HCl solution, *J. Mater. Sci. Technol*., 2013, **29**, no. 9, 884–892. doi: 10.1016/j.jmst.2013.06.006
13. N. Baby and P. Manjula, Quantum chemical analysis of the inhibitive effect of pyrimidine derivative on mild steel in neutral aqueous media, *Int. J. Innov. Res. Sci. Eng. Tech*., 2016, **5**, no. 3, 3977–3985. doi: 10.15680/IJIRSET.2016.0503154
14. K.F. Khaled, K. Babic-Samardzija and N. Hackerman, Theoretical study of the structural effects of polymethylene amines on corrosion inhibition of iron in acid solutions, *Electrochim. Acta*, 2005, **50**, no. 12, 2515–2520, doi: 10.1016/j.electacta.2004.10.079
15. H.Z.M. Al-Sawaad, Thermodynamic and quantum chemistry study for dimethylol-5-methyl hydantoin and its derivatives as corrosion inhibitors for carbon steel N-80 in raw water (cooling water system), *J. Mater. Environ. Sci*., 2011, **2**, no. 2, 128–147.
16. M. Abdallah, M.A. Hegazy, H. Ahmed, A.S. Al-Gorair, H. Hawsawi, M. Morad, F. Benhiba, I. Warad and A. Zarrouk, Appraisal of synthetic cationic Gemini surfactants as highly efficient inhibitors for carbon steel in the acidization of oil and gas wells: an experimental and computational approach, *RSC Adv*., 2022, **12**, no. 27, 17050–17064. doi: 10.1039/d2ra02603a
17. T.K. Sarkar, M. Yadav and I.B. Obot, Mechanistic evaluation of adsorption and corrosion inhibition capabilities of novel indoline compounds for oil well/tubing steel in 15% HCl, *Chem. Eng. J*., 2022, **431**, 133481. doi: 10.1016/j.cej.2021.133481
18. M.T. Finjan, Preparation, identification, and evaluation of some Gemini surfactants derivative from ethylenediamine tetraacetic acid, M.Sc. Thesis, 2011, University of Basrah, Iraq.
19. V. Pinto, G.M. Pinto, L.D. Kateel and A. Thomas, Green approach to corrosion inhibition of mild steel in hydrochloric acid using extract from the pericarp of the fruit *Tamarindus indica* (Tamarind), *Biointerface Res. Appl. Chem*., 2023, **13**, no. 6, 544. doi: 10.33263/BRIAC136.544
20. O.S. Yadav, S. Kumar, G. Kaur and G. Singh, Corrosion resistance of mild steel in acid solution in the presence of [4-methoxy-6-methyl-pyrimidin-2yl] pyridine-2 ylmethylene- amine as corrosion inhibitor, *Heterocycl. Lett*., 2014, **4**, no. 2, 251–266.
21. M.J. Meften and A.A. Kadhim, Synthesis of 5-benzyl-5-((5-nitropyridin-3yl)methyl)-1,3,5-dithiazinan-5-ium through one-pot reactions, characterization and study as a corrosion retardant in high salinity oil fields, *J. Basrah Res. (Sci.)*., 2023, **49**, no. 2, 140–126. doi: 10.56714/bjrs.49.2.12
22. S. Fu, X. Yang, Y. Peng, Q. Wang, Q. Sun, J. Zhang, X. Wang, Z. Liang and J. Li, Corrosion Behaviors of Tetrasodium Iminodisuccinate (IDS) as an Environmentally Friendly Inhibitor: Experimental and Theoretical Studies, *Coatings*, 2023, **13**, no.3, 613. doi: 10.3390/coatings13030613

23. C.M. Méndez, C.A. Gervasi, G. Pozzi and A.E. Ares, Corrosion inhibition of aluminum in acidic solution by *ilex paraguariensis* (Yerba Mate) extract as a green inhibitor, *Coatings*, 2023, **13**, no. 2, 434. doi: 10.3390/coatings13020434
24. K. Shalabi, H.M. Abd El-Lateef, M.M. Hammouda, A.M.A. Osman, A.H. Tantawy and M.A. Abo-Riya, Perspectives on corrosion inhibition features of novel synthesized Gemini-fluorinated cationic surfactants bearing varied Spacers for acid pickling of X60-steel: practical, and in silico calculations, *Materials*, 2023, **16**, no. 14, 5192. doi: 10.3390/ma16145192
25. H.A. Abdullah, R.A. Anaee, A.A. Khadom, A.T. Abd Ali, A.H. Malik and M.M. Kadhim, Experimental and theoretical assessments of the chamomile flower extract as a green corrosion inhibitor for aluminum in artificial seawater, *Results Chem.*, 2023, **6**, 101035. doi: 10.1016/j.rechem.2023.101035
26. A. Toghan, A. Fawzy, A.I. Alakhras, M.M.S. Sanad, M. Khairy and A.A. Farag, Correlating Experimental with Theoretical Studies for a New Ionic Liquid for Inhibiting Corrosion of Carbon Steel during Oil Well Acidification, *Metals*, 2023, **13**, no. 5, 862. doi: 10.3390/met13050862
27. R.D. Pruthviraj, A.S.S. Kumar, A. Sudhakara and S. Ramesha, Inhibitory Impact of Oxacillin on Corrosion by Using 1 M Hydrochloric Acid Solution, *Pharma Chem.*, 2022, **14**, no. 10, 1–8. doi: 10.4172/0975413-X.14.10.1-8
28. K. Alaoui, Y. El Kacimi, M. Galai, H. Serrar, R. Touir, S. Kaya, C. Kaya and M. Ebn Touhami, New triazepine carboxylate derivatives: correlation between corrosion inhibition property and chemical structure, *Int. J. Ind. Chem.*, 2020, **11**, 23–42. doi: 10.1007/s40090-019-00199-5
29. N. Nnaji, N. Nwaji and T. Nyokong, Electrodeposited Benzothiazole Phthalocyanines for Corrosion Inhibition of Aluminium in Acidic Medium, *Int. J. Electrochem.*, 2020, **2020**, 1–11. doi: 10.1155/2020/8892559
30. M. Mouayad and M.S. Shihab, Pyridinium bromide derivatives as corrosion inhibitors for mild Steel in 1 M, *Egypt. J. Chem.*, 2023, **66**, no. 2, 63–72. doi: 10.21608/ejchem.2022.126742.5625
31. A. Toghan, M. Khairy, M. Huang and A.A. Farag, Electrochemical, chemical and theoretical exploration of the corrosion inhibition of carbon steel with new imidazole-carboxamide derivatives in an acidic environment, *Int. J. Electrochem. Sci.*, 2023, **18**, no. 3, 100072. doi: 10.1016/j.ijoes.2023.100072
32. C.U.D. Eze, N.A. Madueke, N.B. Iroha, N.J. Maduelosi, L.A. Nnanna, V.C. Anadebe and A.A. Chokor, Adsorption and inhibition study of N-(5-methoxy-2-hydroxybenzylidene) isonicotinohydrazide Schiff base on copper corrosion in 3.5% NaCl, *Egypt. J. Pet.*, 2022, **31**, no. 2, 31–37. doi: 10.1016/j.ejpe.2022.05.001
33. L.B. Furtado, G.B. Leoni, R.C. Nascimento, P.H.C. Santos, F.J.F.S. Henrique, M.O.C. Guimarães and S.L.C. Brasil, Experimental and Theoretical Studies of Tailor-made Schiff Bases as Corrosion Inhibitors for Carbon Steel in HCl, *Mat. Res.*, 2023, **26**, 1–18. doi: 10.1590/1980-5373-MR-2022-0398

34. A. Toghan, A. Fawzy, A.I. Alakhras, M.M.S. Sanad, M. Khairy and A.A. Farag, Correlating Experimental with Theoretical Studies for a New Ionic Liquid for Inhibiting Corrosion of Carbon Steel during Oil Well Acidification, *Metals*, 2023, **13**, no. 5, 862. doi: 10.3390/met13050862
35. N.A. Othman, M.M. Ali, N.S. Samsi, F. Salim, D. Panuh, M.K. Yaakob, Z. Embong, A.S. Sauri, N.N.C. Isa and N.Z.N. Hashim, Environmentally conscience corrosion inhibitors for mild steel in corrosive hydrochloric acid solution by *Uncaria Cordata* extract: experimental and theoretical studies, *J. Adhes. Sci. Technol*., 2023, **37**, no. 23, 1–29. doi: 10.1080/01694243.2023.2196905
36. K. Azizollah, Synergistic Effect Between Oleic Imidazoline and 2-Mercaptobenzimidazole for Increasing the Corrosion Inhibition Performance in Carbon Steel Samples, *Iran. J. Chem. Chem. Eng*., 2023, **42**, no. 1, 1–16. doi: 10.30492/ijcce.2022.546098.5091
37. M.J. Meften, W.A. Radhi and A.N. Abulhail, Molecular structure and electronic characteristics study of imidazole and dioxol derivatives as corrosion inhibitors. A quantum methodology investigation, *J. Basrah Res. (Sci.)*., 2018, **36**, no. 1, 1–29. doi: 10.29072/basjs.2018302
38. L. Feng, C. Yin, H. Zhang, Y. Li, X. Song, Q. Chen and H. Liu, Cationic Gemini surfactants with a bipyridyl spacer as corrosion inhibitors for carbon steel, *ACS Omega*, 2018, **3**, no. 12, 18990–18999. doi: 10.1021/acsomega.8b03043
39. H. Lgaz, R. Salghi, M. Larouj, M. Elfaydy, S. Jodeh, Z. Rouifi, B. Lakhrissi and H. Oudda, Experimental, theoretical and Monte Carlo simulation of quinoline derivative as effective corrosion inhibitor for mild steel in 1 M HCl, *J. Mater. Environ. Sci*., 2016, **7**, no. 12, 4471–4488.
40. M. Barbouchi, B. Benzidia, A. Ghaleb, A. Aouidate, M. El Idrissi and M. Choukrad, Theoretical and Experimental Studies of Lentisk Leaf Extract as Green Corrosion Inhibitor for Iron in Chloride Media, *Biointerface Res. Appl. Chem*., 2023, **13**, no. 6, 557. doi: 10.33263/BRIAC136.557
41. S.A. Abd El-Maksoud, F.I. El-Dossoki, M. Abd-Elhamed and A.A. Farag, Some new synthesized gemini cationic surfactants as corrosion inhibitors for carbon steel in hydrochloric acid solution, *J. Bio Tribo Corros*., 2023, **9**, no. 71, 1–51. doi: 10.21203/rs.3.rs-2679512/v1
42. S.N. Dalhatu, K.A. Modu, A.A. Mahmoud, Z.U. Zango, A.B. Umar, F. Usman, J.O. Dennis, A. Alsadig, K.H. Ibnaouf and O.A. Aldaghri, L-Arginine Grafted Chitosan as Corrosion Inhibitor for Mild Steel Protection, *Polymers*, 2023, **15**, no. 2, 398. doi: 10.3390/polym15020398
43. S. Fu, X. Yang, Y. Peng, Q. Wang, Q. Sun, J. Zhang, X. Wang, Z. Liang and J. Li, Corrosion behaviors of tetrasodium iminodisuccinate (IDS) as an environmentally friendly inhibitor: experimental and theoretical studies, *Coatings*, 2023, **13**, no. 3, 613. doi: 10.3390/coatings13030613

44. S. Tanwer and S.K. Shukla, Cefuroxime: A Potential corrosion inhibitor for mild steel in sulphuric acid medium, *Prog. Color, Color. Coat*., 2023, **16**, no. 2, 125–138. doi: 10.30509/pccc.2022.166974.1165
45. B. Delley, DMol^3 DFT studies: from molecules and molecular environments to surfaces and solids, *Comput. Mater. Sci*., 2000, **17**, no. 2–4, 122–126. doi: 10.1016/S0927-0256(00)00008-2
46. R. Jalab, M.A. Saad, M.H. Sliem, A.M. Abdullah and I.A. Hussein, An Eco-Friendly Quaternary Ammonium Salt as a Corrosion Inhibitor for Carbon Steel in 5 M HCl Solution: Theoretical and Experimental Investigation, *Molecules*, 2022, **27**, no. 19, 6414. doi: 10.3390/molecules27196414
47. L.B. Furtado, G.B. Leoni, R.C. Nascimento, P.H.C. Santos, F.J.F.S. Henrique, M.J.O.C. Guimarães and S.L.D.C. Brasil, Experimental and Theoretical Studies of Tailor-made Schiff Bases as Corrosion Inhibitors for Carbon Steel in HCl, *Mat. Res*., 2023, **26**, 1–18. doi: 10.1590/1980-5373-MR-2022-0398
48. M.S. Numin, K. Jumbri, K.E. Kee, A. Hassan, N. Borhan and J. Matmin, DFT Calculation and MD Simulation Studies on Gemini Surfactant Corrosion Inhibitor in Acetic Acid Media, *Polymers*, 2023, **15**, no. 9, 2155. doi: 10.3390/polym15092155
49. A. Mohammed, A.Y.I. Rubaye, W.K. Al-Azzawi and A. Alamiery, Investigation of the corrosion inhibition properties of 4-cyclohexyl-3 thiosemicarbazide on mild steel in 1 M HCl solution, *Prog. Color, Color. Coat*., 2023, **16**, no. 4, 347–359. doi: 10.30509/pccc.2023.167126.1212
50. O.E. Oyeneyin, N.D. Ojo, N. Ipinloju, E.B. Agbafa and A.V. Emmanuel, Investigation of the corrosion inhibition potentials of some 2-(4-(substituted) arylidene)-1H-indene-1,3-dione derivatives: density functional theory and molecular dynamics simulation, *BJBAS*, 2022, **11**, no. 132, 1–14. doi: 10.1186/s43088-022-00313-0
51. M.J. Meften, Preparation of novel compounds, characterization and studying experimentally and theoretically as inhibitors through thermodynamic and quantum chemistry, *Eur. J. Chem*., 2017, **8**, no. 3, 229–239. doi: 10.5155/eurjchem.8.3.229-239.1589
52. S. Hadisaputra, A.A. Purwoko, L.R.T. Savalas, N. Prasetyo, E. Yuanita and S. Hamdiani, Quantum chemical and monte carlo simulation studies on inhibition performance of caffeine and its derivatives against corrosion of copper, *Coatings*, 2020, **10**, no. 11, 1086. doi: 10.3390/coatings10111086
53. M. Adardour, M. Lasri, M.A. Lahcen, M. Maatallah, R. Idouhli, M.M. Alanazi, S. Lahmidi, A. Abouelfida, J.T. Mague and A. Baouid, Exploring the Efficacy of Benzimidazolone Derivative as Corrosion Inhibitors for Copper in a 3.5 wt.% NaCl Solution: A Comprehensive Experimental and Theoretical Investigation, *Molecules*, 2023, **28**, no. 19, 6948. doi: 10.3390/molecules28196948
54. T.S. Reddy, K. Raja, K.N. Teja reddy and S.B.M. Surya, Synthesis, DFT, ADME and docking studies of Homoegonol and Egonol as potential inhibitors of COVID-19 main protease (6LU7), *Results Chem*., 2023, **6**, 101084. doi: 10.1016/j.rechem.2023.101084

55. H. Messaoudi, F. Djazi, M. Litim, B. Keskin, M. Slimane and D. Bekhiti, Surface analysis and adsorption behavior of caffeine as an environmentally friendly corrosion inhibitor at the copper/aqueous chloride solution interface, *J. Adhes. Sci. Technol*., 2020, **34**, no. 20, 2216–2244. doi: 10.1080/01694243.2020.1756156
56. K.F. Khaled and M.A. Amin, Dry and wet lab studies for some benzotriazole derivatives as possible corrosion inhibitors for copper in 1.0 M HNO_3, *Corros. Sci*., 2009, **51**, no. 9, 2098–2106. doi: 10.1016/j.corsci.2009.05.038
57. R. Oukhrib, Y. Abdellaoui, A. Berisha, H.A. Oualid, J. Halili, K. Jusufi, M.A. El Had, H. Bourzi, S. El Issami, F. Ali Asmary, V.S. Parmar and C. Len, DFT Monte Carlo and molecular dynamics simulations for the prediction of corrosion inhibition efficiency of novel pyrazolyl nucleosides on Cu(111) surface in acidic media, *Sci. Rep*., 2021, **11**, no. 3771, 1–18. doi: 10.1038/s41598-021-82927-5
58. A.I. Ikeuba, J.E. Ntibi, P.C. Okafor, B.I. Ita, A.U. Agobi, F.C. Asogwa, B.J. Omang, E.A. Eno, H. Loius, S.A. Adalikwu, B.A. Abiola, F.E. Abeng and N.A. Abang, Kinetic and thermodynamic evaluation of azithromycin as a green corrosion inhibitor during acid cleaning process of mild steel using an experimental and theoretical approach, *Results Chem*., 2023, **5**, 100909. doi: 10.1016/j.rechem.2023.100909.
59. A.K. Kushwaha, M.R. Sahoo, M. Ray, D. Das, S. Nayak, A. Maity, K. Sarkar, A.N. Bhagat, A.R. Pal, T.K. Rout and S.K. Nayak, Functional pyromellitic diimide as a corrosion inhibitor for galvanized steel: An Atomic-Scale Engineering, *ACS Omega*, 2022, **7**, no. 31, 27116–27125. doi: 10.1021/acsomega.2c01299
60. P. Han, Y. He, C. Chen, H. Yu, F. Liu, H. Yang, Y. Ma and Y. Zheng, Study on synergistic mechanism of inhibitor mixture based on electron transfer behavior, *Sci. Rep*., 2016, **6**. doi: 10.1038/srep33252
61. A.A. Kadhim, H. Sedghi and J.M.K. Al-zyadi, Investigation of structural, electronic, and optical properties of bulk and monolayer for new material CrS under electric field effect, *J. Magn. Magn. Mater*., 2024, **603**, 172276. doi: 10.1016/j.jmmm.2024.172276
62. A.H. Al-Moubaraki, A. Chaouiki, J.M. Alahmari, W.A. Al-hammadi, E.A. Noor, A.A. Al-Ghamdi and Y.G. Ko, Development of Natural Plant Extracts as Sustainable Inhibitors for Efficient Protection of Mild Steel: Experimental and First-Principles Multi-Level Computational Methods, *Materials*, 2022, **15**, no. 23, 8688. doi: 10.3390/ma15238688
63. A. Nasser, N.M. EL Basiony, M.A. Migahed, H.M. Abd-El-Bary and T.A. Mohamed, Experimental and theoretical insights into synthesized Gemini corrosion inhibitor for X65-steel in 1 M HCl, *Egypt. J. Chem*., 2022, **65**, no. 13, 845–867. doi: 10.21608/EJCHEM.2022.152233.6594

♦ ♦ ♦